Available online at www.sciencedirect.com

ScienceDirect

Ceramics International 40 (2014) 3841–3846

CERAMICS INTERNATIONAL

www.elsevier.com/locate/ceramint

Structural, magnetic and dielectric behavior of $Mg_{1-x}Ca_xNi_yFe_{2-y}O_4$ nano-ferrites synthesized by the micro-emulsion method

Rajjab Ali[a], Muhammad Azhar Khan[b], Azhar Mahmood[a], Adeel Hussain Chughtai[c], Amber Sultan[d], Muhammad Shahid[e], Muhammad Ishaq[f], Muhammad Farooq Warsi[a,*]

[a]Department of Chemistry, The Islamia University of Bahawalpur, Bahawalpur 63100, Pakistan
[b]Department of Physics, The Islamia University of Bahawalpur, Bahawalpur 63100, Pakistan
[c]Institute of Chemical Sciences, Bahauddin Zakaryia University, Multan 6100, Pakistan
[d]Quaid-e-Azam Medical College, Bahawalpur 63100, Pakistan
[e]Physics Research Division, Institute of Basic Sciences, Department of Energy Science, Sungkyunkwan University, Suwon 440-746, South Korea
[f]Department of Chemistry, Quaid-i-Azam University, Islamabad 45320, Pakistan

Received 25 July 2013; received in revised form 6 August 2013; accepted 6 August 2013
Available online 14 August 2013

Abstract

Ca–Ni co-substituted samples of nanocrystalline spinel ferrites with chemical formula $Mg_{1-x}Ca_xNi_yFe_{2-y}O_4$ ($x=0.0$–0.6, $y=0.0$–1.2) were synthesized by the micro-emulsion method and were annealed at 700 °C for 7 h. The synthesized samples were characterized by x-ray diffraction (XRD), Fourier transform infrared (FTIR) spectroscopy, vibrating sample magnetometry (VSM) and dielectric measurements. The XRD and FTIR analysis reveals that single phase samples can be achieved by substituting Ca and Ni ions at Mg and Fe sites respectively in cubic spinel nano-ferrites. The crystallite size of the synthesized samples was found in the range 29–45 nm. The saturation magnetization (M_s) increases from 9.84 to 24.99 emu/g up to $x=0.2$, $y=0.4$ and then decreases, while the coercivity (H_c) increases continuously from 94 to 153 Oe with the increase in dopants concentration. The dielectric properties of these nano materials were also studied at room temperature in the frequency range 100 MHz to 3 GHz. The dielectric parameters were found to decrease with the increased Ca–Ni concentration. Further the peaking behavior was observed beyond 1.5 GHz. The frequency dependent dielectric properties of all the samples have been explained qualitatively on the basis of the Maxwell–Wagner two-layer model according to Koop's phenomenological theory. The enhanced magnetic parameters and reduced dielectric properties make the synthesized materials suitable for switching and high frequency applications, respectively.
© 2013 Elsevier Ltd and Techna Group S.r.l. All rights reserved.

Keywords: C. Dielectric properties; C. Magnetic properties; Nano-ferrites; Spectral analysis; X-ray diffraction

1. Introduction

The synthesis and characterization of nanocrystalline spinel ferrites is still continue to be an intense area of research owing to their versatility in finding a large number of technological applications over a wide frequency range due to their low cost and high electromagnetic performance [1–3]. Nano-ferrites play an important role in modern industrial society. These are used in advanced electronics because of their multi-functional features and potential applications in transducers, actuators, sensors, microwave and computer technology etc. The structural, magnetic and electrical properties of nano-ferrites are influenced by composition and method of fabrication. Several chemical methods have been employed for the fabrication of nano-ferrites [4]. These include sol gel [5,6], citrate precursor [7], co-precipitation [8,9], microwave assisted hydrothermal [10], reverse micelle [11] etc. These different routes produce different crystallite sizes based on the ease and reproducibility. A close review of literature evokes that many research groups so far have concentrated on simple rather than

*Corresponding author. Tel.: +92 62 9255473; fax: +92 62 9255474.
E-mail addresses: Farooq.warsi@iub.edu.pk, farooqsi_warsi@yahoo.com (M.F. Warsi).

0272-8842/$ - see front matter © 2013 Elsevier Ltd and Techna Group S.r.l. All rights reserved.
http://dx.doi.org/10.1016/j.ceramint.2013.08.024

complex ferrite system perhaps due to having better insight into the behavior of these materials in the nano regime. Modifying the chemical composition of nano-ferrites, one can possibly enhance their properties [12]. $MgFe_2O_4$ ferrite is a soft magnetic material having partial inverse spinel structure and is regarded as important candidate of the spinel ferrite family [13]. The distribution of the cations among the octahedral and tetrahedral sites of magnesium ferrites affects the structural and electromagnetic properties. Several cations such Dy^{3+}, Ca^{2+}, Cd^{2+}, In^{3+} and Al-Cr have been substituted for either Mg^{2+} or Fe^{3+} in order to obtain optimized magnetic and dielectric properties of nano-ferrites [14–17].

The aim of the present work is to fabricate nanocrystalline materials and to enhance the magnetic (saturation magnetization, coercivity and remanance) properties and dielectric (dielectric constant, complex dielectric constant, dielectric loss) properties to make these nano materials suitable for switching and high frequency (GHz) devices applications.

2. Materials and methods

A series of single phase nano-spinel ferrites with composition $Mg_{1-x}Ca_xNi_yFe_{2-y}O_4$ (x=0, 0.2,0.4,0.6, y=0, 0.4, 0.8, 1.2) were prepared using the micro-emulsion method [8,18]. Following chemicals were used as received without any further purification: $Fe(NO_3)_2 \cdot 9H_2O$ (Sigma-Aldrich, 98%), $CaCl_2 \cdot 2H_2O$ (Sigma-Aldrich, 98%), $MgSO_4 \cdot 7H_2O$ (Sigma-Aldrich, 98%), $NiCl_2 \cdot 6H_2O$ (Sigma-Aldrich, 99%), cetlytrimethylammonium bromide (CTAB) (Fluka, 98%) and aqueous NH_3 (BDH 35%). Required volumes of metal salts solutions of concentrations 0.15 M and 0.3 M were taken in beakers and then stirring was done at 50–60 °C using a magnetic stirrer with controlled thermostat. Aqueous solution of CTAB (0.675 M) was added to the stirred solution of various metal salts. The pH value was maintained (~9–10) with the help of aqueous ammonia solution (~2 M).The reaction mixtures of all samples were further stirred for ~5 h. The precipitates formed by the addition of aqueous ammonia were washed with deionised water until the pH reduced to neutral level (~7) and then washed with methanol to remove any organic based impurity. Water was evaporated in the oven at 100 °C, and then all the samples were subjected to annealing at 700 °C for 7 h in a temperature controlled muffle furnace Vulcan A-550. The obtained materials were grinded into powder form and were characterized by various techniques.

XRD patterns for "$Mg_{1-x}Ca_xNi_yFe_{2-y}O_4$" ($x$=0, 0.2,0.4, 0.6, y=0, 0.4, 0.8, 1.2) nano-ferrites were performed on a Philips X' Pert PRO 3040/60 diffractometer with Cu Kα as radiation source to observe the phase formation of synthesized nano materials. FTIR spectra of "$Mg_{1-x}Ca_xNi_yFe_{2-y}O_4$" nano-ferrites were recorded on a Nexus 470 spectrometer in the range of 400–4000 cm^{-1} at 298 K. Magnetic parameters were recorded at a vibrating sample magnetometer VSM Lakeshore-74071 at 298 K. Dielectric properties were studied using a 4287A RF LCR meter in the range of 100 MHz to 3 GHz.

3. Results and discussion

3.1. Structural properties

The x-ray diffraction patterns of $Mg_{1-x}Ca_xNi_yFe_{2-y}O_4$ (x=0.0–0.6, y=0.0–1.2) nano-ferrites reveal the single phase spinel structure without any ambiguous reflection as shown in Fig. 1. The diffraction peaks corresponding to planes (220), (311), (222), (400), (422), (333) and (440) provide a clear evidence for the formation of spinel structure of the ferrite [19]. Experimentally observed '*d*' spacing values and relative intensities of the diffraction peaks are in well agreement with the crystalline cubic spinel form of the magnesium ferrite (JCPDS Card no: 36-0398). The intensities of the (220) and (440) planes are more sensitive to the cations on tetrahedral and octahedral sites respectively [20,21]. As reported earlier Mg^{2+} ions have a strong preference to occupy B sites and partially occupy A sites [22]. The observed intensities of the above two planes are found to decrease by the substitution of Ca^{2+} and Ni^{2+} ions. The decrease in the intensity of the (440) plane indicate that the substitution of Ca^{2+} and Ni^{2+} ion concentration takes place at B-site, i.e. the octahedral site on the (440) plane. The intensity of (220) plane also decreases by the continuous substitution of the substituting ions, which leads to migration of few Fe^{3+} ions from B-sites to A-sites. Hence, it is expected that most of the replacement of substituted ions (Ca^{2+}, Ni^{2+}) occurs on the octahedral sites.

The lattice parameter is obtained by fitting seven diffraction peaks using the standard Nelson–Riley refinement method [23]. The lattice parameter increases linearly with the increase of Ca^{2+} and Ni^{2+} contents. This increase in lattice parameter is due to the larger ionic radius of Ca^{2+} (1.14 Å) and Ni^{2+} (0.69 Å) than those of host cations i.e. Mg^{2+} (0.72 Å) and Fe^{3+} (0.64 Å). No other phase was observed in the XRD patterns, indicating that no chemical transformation occurred during the heat treatment. The XRD patterns indicated that the synthesized powders contain nanosized crystallites. The crystallite

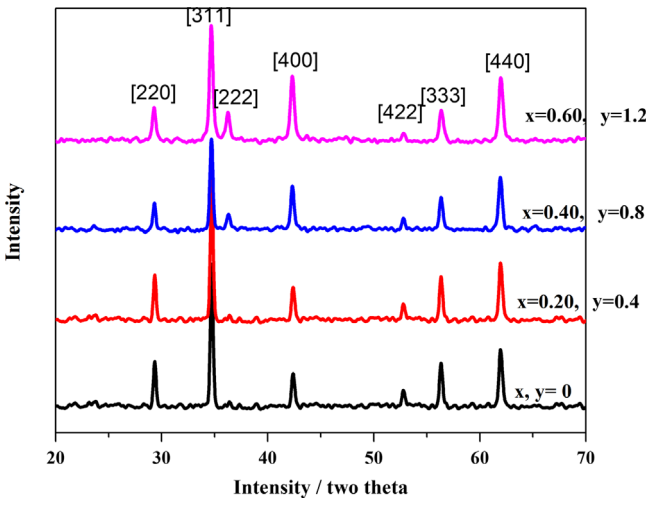

Fig. 1. X-ray diffraction patterns for $Mg_{1-x}Ca_xNi_yFe_{2-y}O_4$ nano-ferrites.

Table 1
Crystallite size (D), lattice parameter (a), cell volume (V_{cell}), x-ray density (ρ_x), measured density (ρ_m) and porosity ($P\%$) of $Mg_{1-x}Ca_xNi_yFe_{2-y}O_4$ (x=0.0–0.6, y=0.0–1.2) nano-ferrites.

Parameters	$x=0$ $y=0$	$x=0.2$ $y=0.4$	$x=0.4$ $y=0.8$	$x=0.8$ $y=1.2$
Lattice constant/a (Å)	8.352	8.353	8.355	8.359
Cell volume/V_{cell} (Å^3)	582.6	582.8	583.2	584
Bulk density/ρ_{bulk} (g cm^{-3})	2.75	2.83	3.01	3.19
X-ray density/$\rho_{x\text{-}ray}$ (g cm^{-3})	3.18	3.26	3.34	3.43
Porosity (%)	13.52	13.19	9.88	6.99
Crystallite size/D (nm)	29	37	42	45

size is estimated by using Scherrer's formula [24]

$$D = \frac{0.9\lambda}{\beta \cos\theta} \tag{3.1}$$

where D is the crystallite size, λ is the wavelength of x-rays (1.54 Å), β is the full width at half maximum, and θ is the angle of diffraction. The average crystallite size (Table 1) of the Ca–Ni substituted samples is found in the range 29–45 nm, which is smaller compared to that synthesized by other method (40–57 nm) reported for spinel ferrites [25]. It has been reported that a crystallite size of <50 nm is desirable for obtaining a suitable signal-to-noise ratio for switching applications [8]. The x-ray density of the samples is calculated by the relation

$$\rho_x = \frac{8M}{Na^3} \tag{3.2}$$

where M is the molecular weight of the sample, N is Avogadro's number and a^3 volume of the cubic unit cell. The measured density is calculated by using the relation

$$\rho_m = \frac{M}{V} = \frac{M}{\pi r^2 t} \tag{3.3}$$

where M is the mass, r is the radius, and t is the thickness of the pellet. Porosity of the samples is determined by using the relation

$$P = \frac{\rho_x - \rho_m}{\rho_x} 100 \tag{3.4}$$

where ρ_x is the x-ray density and ρ_m is the measured density. The x-ray density increases from 3.18 to 3.43 g/cm^3 while porosity varies from 13.52 to 6.99 with the substitution of Ca–Ni contents.

3.2. FTIR studies

Fig. 2 shows the representative room temperature FTIR spectrum of $Mg_{1-x}Ca_xNi_yFe_{2-y}O_4$ nano-ferrites prepared by the micro-emulsion method. The representative spectrum of these as synthesized nano-ferrites obtained manifest absorption peaks located at about 427, 519, 1094, 1211, 1368, 1642, 1733, 2011 and 2361 in the region of 2400–400 cm^{-1}. The absorption peaks 427, 519 (shown in inset) are referred to the intrinsic vibrations of the octahedral and tetrahedral group complexes, which are characteristic features of spinel ferrites [26].

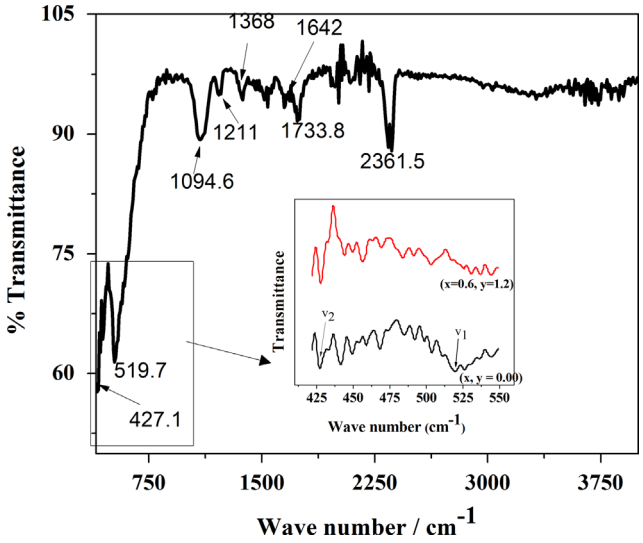

Fig. 2. FTIR spectra for $Mg_{1-x}Ca_xNi_yFe_{2-y}O_4$ (x=0.0, y=0.0) nano-ferrites.

The absorption peaks at 1642 cm^{-1} and 2361 cm^{-1} are ascribed to the absorbed water molecules and adsorbed or atmospheric CO_2 [27]. The absorption peaks 1094 and 1368 are attributed to the deformation of C–H group and carboxylic group [28]. The increase in tetrahedral absorption peak from 519.7 to 556.5 elucidate the drifting of Fe^{3+} ions towards oxygen ions on occupation of tetrahedral sites by Mg^{2+} ions caused by the substitution of Ni–Ca contents on the octahedral sites [29].

3.3. Magnetic properties

The M–H loops for all Ca–Ni co-substituted samples of $Mg_{1-x}Ca_xNi_yFe_{2-y}O_4$ (x=0.0–0.6, y=0.0–1.2) nano-ferrites were measured up to an applied field of 10 kOe and are shown in Fig. 3. The values of saturation magnetization (M_s), coercivity (H_c) and remanence (M_r) are found to be in the range of (9.84–19.89) emu/g, (94.44–153.08) emu/g, (1.32–3.84) O_e respectively.

The squareness ratios for all the samples were also calculated from M_s and M_r data, and the calculated values are listed in Table 2.

The saturation magnetization value observed in the present study (9.84 emu/g) is smaller compared to reported literature [30]. The smaller value of saturation magnetization is owing to the speculated differences in inversion parameter, which indicates the distribution of cations between A-and-B sites of the spinel lattice [31] and the spin disorder in the shell around the core [32]. The anomalous behavior of saturation magnetization has been associated with the magnetic disorder on B-sites caused by the presence of non magnetic calcium cations [33]. The ionic distribution in nanostructured ferrites may be different by a certain degree against their preferences in bulk ferrites and this degree of inversion is dependent on crystallite size. Similar results have been reported in literature [34]. The smaller values of coercivity for all the samples indicate the soft nature of these nano-ferrites. The values of coercivity indicate linear relationship with crystallite size (Fig. 4) and the coercivity variations resemble a typical size dependent behavior [5]. It has been reported earlier that a low value of coercivity is favorable for use in switching applications.

3.4. Dielectric properties

The dielectric properties of ferrites nanoparticles depend upon the method of preparation, chemical composition, particle size and cation distribution. Figs. 5–7 show the frequency dependent dielectric constant, complex dielectric constant and dielectric loss for all the samples respectively studied in the frequency range 100 MHz to 3 GHz.

It can be seen from Fig. 5 that as frequency increases dielectric constant decreases exponentially. The decrease in dielectric constant is rather sharp at low frequency region, as

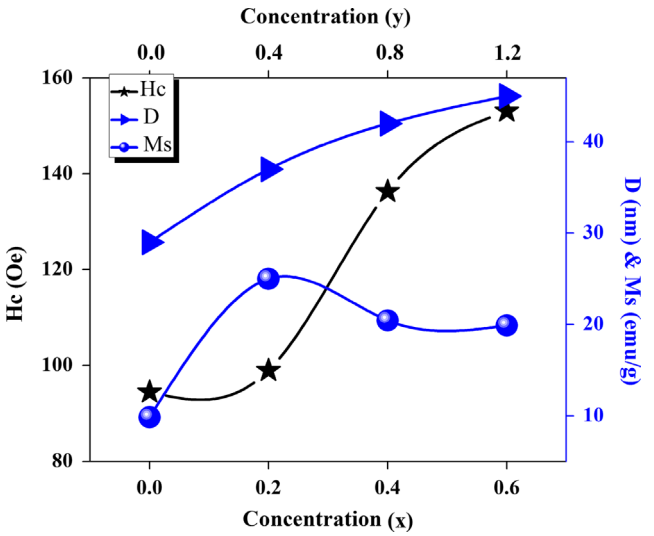

Fig. 4. Variation of saturation magnetization, coercivity and crystallite size for $Mg_{1-x}Ca_xNi_yFe_{2-y}O_4$ nano-ferrites.

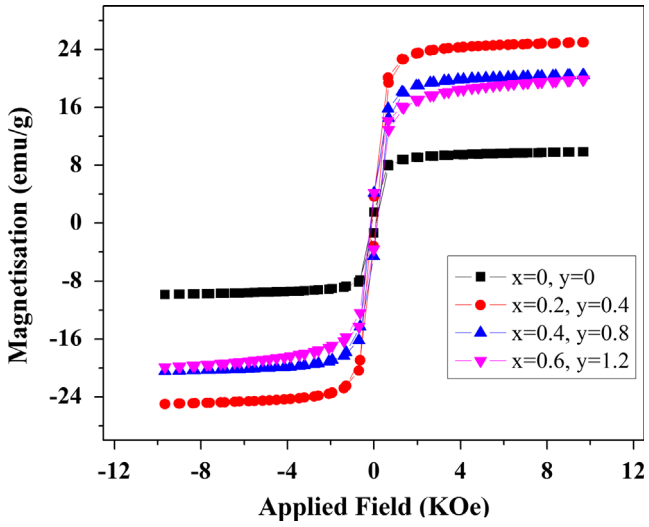

Fig. 3. MH loops of $Mg_{1-x}Ca_xNi_yFe_{2-y}O_4$ nano-ferrites.

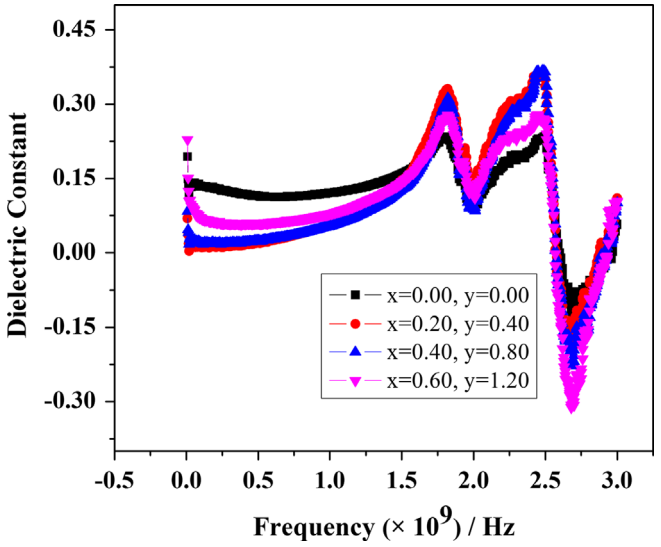

Fig. 5. Dielectric constant $Mg_{1-x}Ca_xNi_yFe_{2-y}O_4$ nano-ferrites.

Table 2
Various magnetic parameters for $Mg_{1-x}Ca_xNi_yFe_{2-y}O_4$ nano-ferrites.

Magnetic parameters	$x=0$ $y=0$	$x=0.2$ $y=0.4$	$x=0.4$ $y=0.8$	$x=0.8$ $y=1.2$
Magnetization (M_s) (emu/g)	9.84	24.99	20.44	19.89
Coercivity (H_c)/G	94.44	98.97	136.32	153.08
Retentivity (M_r) (emu/g)	1.32	3.65	3.83	3.79
$R^2=(M_r/M_s)$	0.13	0.14	0.18	0.19

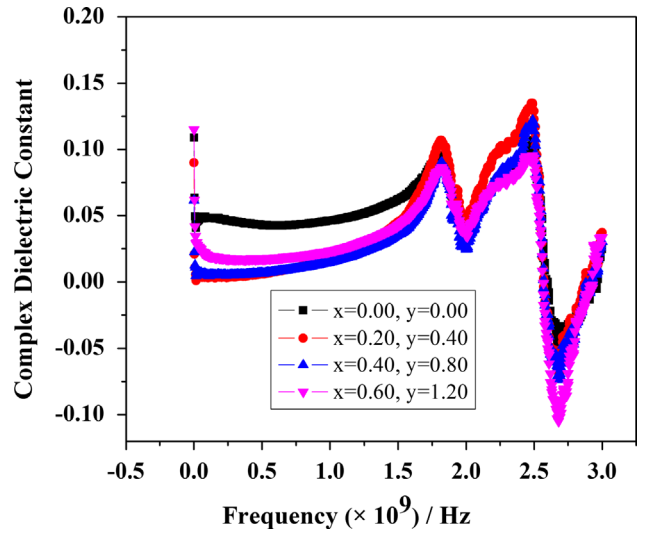

Fig. 6. Complex dielectric constant for $Mg_{1-x}Ca_xNi_yFe_{2-y}O_4$ nano-ferrites.

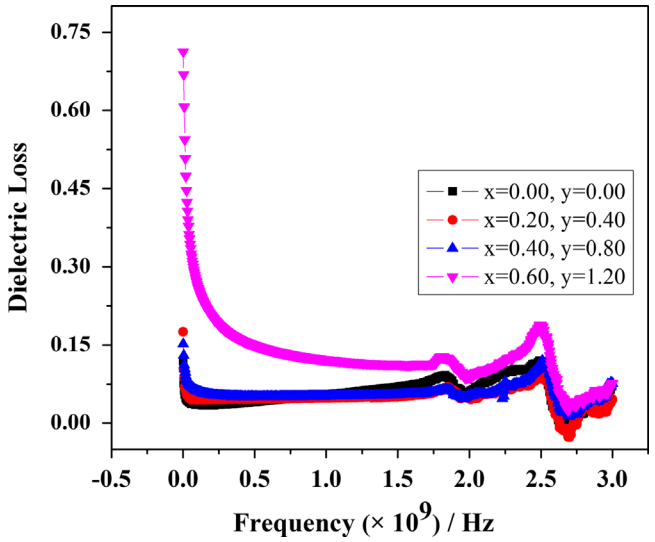

Fig. 7. Dielectric loss as a function of frequency for $Mg_{1-x}Ca_xNi_yFe_{2-y}O_4$ nano-ferrites.

frequency increases it remains almost constant for all the samples under investigation. The variation of dielectric constant with frequency reveals dispersion due to Maxwell–Wagner [35,36] type interfacial polarization and is in agreement to Koop's phenomenological theory [37]. The polarization decreases with increase in frequency and attains constant value over a certain frequency range. Beyond 1.5 GHz, two peaks have been observed around 2 GHz and 2.5 GHz. This type of peaking behavior is observed when the jump frequency of the Fe^{2+} and Fe^{3+} ions is exactly matched to the frequency of applied field.

The decrease in dielectric constant and complex dielectric constant with frequency indicates that mechanism of polarization process in ferrite is similar to that of conducting process. The conduction mechanism in $Mg_{1-x}Ca_xNi_yFe_{2-y}O_4$ spinel ferrites takes place due to electron hopping between Fe^{3+}–Fe^{2+} ions at octahedral (B-site) and hole hopping between Ni^{2+}–Ni^{3+} ions [16]. It is well known that Fe^{3+} ions reside on both A-and B-sites in the spinel lattice and Ni^{2+} ions prefer to occupy B-sites. After the substitution of Ni^{2+} and Ca^{2+} ions by Mg^{2+} and Fe^{3+} ions, some of the Mg^{2+} ions occupy A-sites in the spinel lattice displacing Fe^{3+} ions from there. These displaced Fe^{3+} ions migrate from A-site to B-site and thus increased the concentration of Fe^{3+} ions at B-site increases the hopping conduction which further enhances dielectric polarization at the grain boundary. The probability of occupying Ca^{2+} ions on A-site is very rare owing to the larger ionic radius of Ca^{2+} (1.14 Å). Therefore, the substitution of Ca–Ni enhances the dielectric polarization, consequently the dielectric constant and complex dielectric decrees [38].

The dielectric loss measures the loss of electrical energy from the applied electric field into the samples at different frequencies. The variation of dielectric loss for all Ca–Ni substituted samples is shown in Fig. 7. Fig. 7 indicates that the dielectric loss decreases exponentially with increase in frequency for all the samples under investigation. A maxima in dielectric loss versus frequency appears when frequency of the hopping charge carriers coincides with frequency of the applied alternating field. The maxima in dielectric loss occurs beyond 1.5 GHz. These results were found compatible with already reported results and these materials may be utilized for fabricating the devices working at very high frequencies (GHz) [39].

4. Conclusion

$Mg_{1-x}Ca_xNi_yFe_{2-y}O_4$ nano-ferrites have been successfully synthesized by the micro-emulsion technique. X-ray diffraction patterns of these nano-ferrites and spectral analysis elucidate single phase spinel structure. The average particle size lies in the range 29–45 nm as Ca–Ni contents are incorporated in these nano-ferrites. These crystallites size are small enough to obtain suitable signal-to-noise ratio for switching applications. It is found that the substitution of Ca–Ni in these nano-ferrites leads to an increase in saturation magnetization from 9.84 to 24.99 emu/g up to $x=0.2$ and $y=0.4$, while coercivity increase from 94.44 to 153.08 Oe. The dielectric parameters are enhanced by the incorporation of dopants. The optimized values of dielectric parameters, saturation magnetization and coercivity suggest that the sample with dopant concentration $x=0.2$, $y=0.4$ is suitable in switching and high frequency applications.

Acknowledgments

We are thankful, The Islamia University of Bahawalpur-63100 and Higher Education Commission of Pakistan for financial support under Project no.: PM-IPFP/HRD/HEC/2011/2264, Quaid-e-Azam University Islamabad for XRD and FTIR, Materials Research Laboratory (MRL), University of Peshawar for dielectric measurements, and institute of Solid State Physics (Punjab University, Lahore) for magnetic measurements.

References

[1] A.C. Razzitte, S.E. Jacobo, W.G. Fano, Magnetic properties of MnZn ferrites prepared by soft chemical routes, Journal of Applied Physics 87 (9) (2000) 6232–6234.

[2] V. Babayan, N.E. Kazantseva, I. Sapurina, R. Moučka, J. Vilčáková, J. Stejskal, Magnetoactive feature of in-situ polymerised polyaniline film developed on the surface of manganese–zinc ferrite, Applied Surface Science 258 (19) (2012) 7707–7716.

[3] B. Mušič, M. Drofenik, P. Venturini, A. Žnidaršič, Electromagnetic wave absorption by an organic resin solution based on ferrite particles with a spinel crystal structure, Ceramics International 38 (4) (2012) 2693–2699.

[4] S.M. Patange, S.E. Shirsath, B.G. Toksha, S.S. Jadhav, K.M. Jadhav, Electrical and magnetic properties of Cr^{3+} substituted nanocrystalline nickel ferrite, Journal of Applied Physics 106 (2) (2009) 023914–023917.

[5] M. George, S.S. Nair, A.M. John, P.A. Joy, M.R. Anantharaman, Structural, magnetic and electrical properties of the sol–gel prepared Li0.5Fe2.5O4 fine particles, Journal of Physics D: Applied Physics 39 (5) (2006) 900.

[6] M.J. Nasr Isfahani, M.J. Fesharaki, V. Šepelák, Magnetic behavior of nickel–bismuth ferrite synthesized by a combined sol–gel/thermal method, Ceramics International 39 (2) (2013) 1163–1167.

[7] A.K. Singh, A. Verma, O.P. Thakur, C. Prakash, T.C. Goel, R.G. Mendiratta, Electrical and magnetic properties of Mn–Ni–Zn ferrites processed by citrate precursor method, Materials Letters 57 (5–6) (2003) 1040–1044.

[8] A. Mahmood, M.F. Warsi, M.N. Ashiq, M. Ishaq, Substitution of La and Fe with Dy and Mn in multiferroic La1 − *x*DyxFe1 − *y*Mn*y*O3 nanocrystallites, Journal of Magnetism and Magnetic Materials 327 (0) (2013) 64–70.

[9] A.S. Albuquerque, J.D. Ardisson, W.A.A. Macedo, M.C.M. Alves, Nanosized powders of NiZn ferrite: synthesis, structure, and magnetism, Journal of Applied Physics 87 (9) (2000) 4352–4357.

[10] N. Guskos, J. Typek, G. Zolnierkiewicz, K. Wardal, D. Sibera, U. Narkiewicz, Magnetic resonance study of nanocrystalline ZnO nanopowders doped with Fe_2O_3 obtained by hydrothermal synthesis, Reviews on Advanced Materials Science 129 (2011) 142–149.

[11] A. Ghasemi, A. Paesano, C.F. Cerqueira Machado, Magnetic and reflection loss characteristics of terbium substituted cobalt ferrite nanoparticles/functionalized multi-walled carbon nanotube, IEEE Transactions on Magnetics 48 (4) (2012) 1528–1531.

[12] A.A. Kadam, S.S. Shinde, S.P. Yadav, P.S. Patil, K.Y. Rajpure, Structural, morphological, electrical and magnetic properties of Dy doped Ni–Co substitutional spinel ferrite, Journal of Magnetism and Magnetic Materials 329 (0) (2013) 59–64.

[13] L. Zhang, Y. He, Y. Wu, T. Wu, Photocatalytic degradation of RhB over $MgFe_2O_4/TiO_2$ composite materials, Materials Science and Engineering: B 176 (18) (2011) 1497–1504.

[14] S.I. Park, J.H. Kim, C.G. Kim, C.O. Kim, Effect of substitution elements on magnetization of monodispersed MFe_2O_4 particles, Current Applied Physics 8 (6) (2008) 784–786.

[15] A. Samariya, S.N. Dolia, A.S. Prasad, P.K. Sharma, S.P. Pareek, M.S. Dhawan, S. Kumar, Size dependent structural and magnetic behaviour of $CaFe_2O_4$, Current Applied Physics 13 (5) (2013) 830–835.

[16] K.M. Batoo, S. Kumar, C.G. Lee, Alimuddin, influence of Al doping on electrical properties of Ni–Cd nano ferrites, Current Applied Physics 9 (4) (2009) 826–832.

[17] S.S. Suryawanshi, V.V. Deshpande, U.B. Deshmukh, S.M. Kabur, N.D. Chaudhari, S.R. Sawant, XRD analysis and bulk magnetic properties of Al^{3+} substituted Cu–Cd ferrites, Materials Chemistry and Physics 59 (3) (1999) 199–203.

[18] S. Kumar, V. Singh, S. Aggarwal, U.K. Mandal, R.K. Kotnala, Synthesis of nanocrystalline Ni0.5Zn0.5Fe2O4 ferrite and study of its magnetic behavior at different temperatures, Materials Science and Engineering: B 166 (1) (2010) 76–82.

[19] W.B. Cross, L. Affleck, M.V. Kuznetsov, I.P. Parkin, Q.A. Pankhurst, Self-propagating high-temperature synthesis of ferrites MFe_2O_4 (M = Mg, Ba, Co, Ni, Cu, Zn); reactions in an external magnetic field, Journal of Materials Chemistry 9 (10) (1999) 2545–2552.

[20] B.P. Ladgaonkar, A.S. Vaingankar, X-ray diffraction investigation of cation distribution in $Cd_xCu_{1-x}Fe_2O_4$ ferrite system, Materials Chemistry and Physics 56 (3) (1998) 280–283.

[21] C.S. Narasimhan, C.S. Swamy, Studies on the solid state properties of the solid solution system $MgAl_2 - xFexO_4$, Physica Status Solidi A 59 (2) (1980) 817–826.

[22] R.G. Kulkarni, H.H. Joshi, The magnetic properties of the Mg–Zn ferrite system by Mössbauer spectroscopy, Solid State Communications 53 (11) (1985) 1005–1008.

[23] B.D. Cullity, Elements of X-Ray Diffraction, Elements of X-Ray Diffraction, Addison Wesley, USA, 1978.

[24] M.G. Ferreira da Silva, M.A. Valente, Magnesium ferrite nanoparticles inserted in a glass matrix—Microstructure and magnetic properties, Materials Chemistry and Physics 132 (2–3) (2012) 264–272.

[25] S. Mishra, T.K. Kundu, K.C. Barick, D. Bahadur, D. Chakravorty, Preparation of nanocrystalline $MnFe_2O_4$ by doping with Ti^{4+} ions using solid-state reaction route, Journal of Magnetism and Magnetic Materials 307 (2) (2006) 222–226.

[26] B.K. Labde, M.C. Sable, N.R. Shamkuwar, Structural and infra-red studies of Ni1+*x*Pb*x*Fe2 − 2*x*O4 system, Materials Letters 57 (11) (2003) 1651–1655.

[27] X. Ma, H. Sun, H. He, M. Zheng, Competitive reaction during decomposition of hexachlorobenzene over ultrafine Ca–Fe composite oxide catalyst, Catalysis Letters 119 (1–2) (2007) 142–147.

[28] Z. Yue, L. Li, J. Zhou, H. Zhang, Z. Gui, Preparation and characterization of NiCuZn ferrite nanocrystalline powders by auto-combustion of nitrate–citrate gels, Materials Science and Engineering: B 64 (1) (1999) 68–72.

[29] M. Mouallem-Bahout, S. Bertrand, O. Peña, Synthesis and characterization of Zn1 − *x*Ni*x*Fe$_2$O$_4$ spinels prepared by a citrate precursor, Journal of Solid State Chemistry 178 (4) (2005) 1080–1086.

[30] M.A. Khan, M.U. Islam, M. Ishaque, I.Z. Rahman, Effect of Tb substitution on structural, magnetic and electrical properties of magnesium ferrites, Ceramics International 37 (7) (2011) 2519–2526.

[31] J.P. Chen, C.M. Sorensen, K.J. Klabunde, G.C. Hadjipanayis, E. Devlin, A. Kostikas, Size-dependent magnetic properties of MnFe_{2}O_{4} fine particles synthesized by coprecipitation, Physical Review B 54 (13) (1996) 9288–9296.

[32] B.K. Jang, Y. Okuhara, H. Matsubara, Electrical resistance of Al_2O_3 fiber reinforced RuO_2/glass hybrid composites during tensile loading, Journal of Materials Science 39 (7) (2004) 2573–2575.

[33] J. Chandradass, A.H. Jadhav, K.H. Kim, H. Kim, Influence of processing methodology on the structural and magnetic behavior of $MgFe_2O_4$ nanopowders, Journal of Alloys and Compounds 517 (0) (2012) 164–169.

[34] K. Maaz, A. Mumtaz, S.K. Hasanain, M.F. Bertino, Temperature dependent coercivity and magnetization of nickel ferrite nanoparticles, Journal of Magnetism and Magnetic Materials 322 (15) (2010) 2199–2202.

[35] J.C. Maxwell, Electricity and Magnetism, Oxford University Press, New York, 1973.

[36] K.W. Wagner, The distribution of relaxation times in typical dielectrics, Annals of Physics\ 40 (1973) 817–819.

[37] C.G. Koops, On the dispersion of resistivity and dielectric constant of some semiconductors at audiofrequencies, Physical Review 83 (1) (1951) 121–124.

[38] M.A. El Hiti, Dielectric behavior and AC electrical conductivity of Zn-substituted Ni–Mg ferrites, Journal of Magnetism and Magnetic Materials 164 (1–2) (1996) 187–196.

[39] M.A. Dar, V. Verma, S.P. Gairola, W.A. Siddiqui, R.K. Singh, R.K. Kotnala, Low dielectric loss of Mg doped Ni–Cu–Zn nano-ferrites for power applications, Applied Surface Science 258 (14) (2012) 5342–5347.